# Identifying Mechanisms of Resistance by Circulating Tumor DNA in EVOLVE, a Phase II Trial of Cediranib Plus Olaparib for Ovarian Cancer at Time of PARP Inhibitor Progression

Stephanie Lheureux[1,2], Stephenie D. Prokopec[1], Leslie E. Oldfield[1], Eduardo Gonzalez-Ochoa[1], Jeffrey P. Bruce[1], Derek Wong[1], Arnavaz Danesh[1], Dax Torti[3], Jonathan Torchia[3], Alexander Fortuna[3], Sharanjit Singh[3], Matthew Irving[3], Kayla Marsh[3], Bernard Lam[3], Vanessa Speers[1], Aleksandra Yosifova[1], Ana Oaknin[4], Ainhoa Madariaga[1], Neesha C. Dhani[1,2], Valerie Bowering[1], Amit M. Oza[1,2], and Trevor J. Pugh[1,3,5]

## ABSTRACT

**Purpose:** To evaluate the use of blood cell–free DNA (cfDNA) to identify emerging mechanisms of resistance to PARP inhibitors (PARPi) in high-grade serous ovarian cancer (HGSOC).

**Experimental Design:** We used targeted sequencing (TS) to analyze 78 longitudinal cfDNA samples collected from 30 patients with HGSOC enrolled in a phase II clinical trial evaluating cediranib (VEGF inhibitor) plus olaparib (PARPi) after progression on PARPi alone. cfDNA was collected at baseline, before treatment cycle 2, and at end of treatment. These were compared with whole-exome sequencing (WES) of baseline tumor tissues.

**Results:** At baseline (time of initial PARPi progression), cfDNA tumor fractions were 0.2% to 67% (median, 3.25%), and patients with high ctDNA levels (>15%) had a higher tumor burden (sum of target lesions; $P = 0.043$). Across all timepoints, cfDNA detected 74.4% of mutations known from prior tumor WES, including three of five expected *BRCA1/2* reversion mutations. In addition, cfDNA identified 10 novel mutations not detected by WES, including seven *TP53* mutations annotated as pathogenic by ClinVar. cfDNA fragmentation analysis attributed five of these novel *TP53* mutations to clonal hematopoiesis of indeterminate potential (CHIP). At baseline, samples with significant differences in mutant fragment size distribution had shorter time to progression ($P = 0.001$).

**Conclusions:** Longitudinal testing of cfDNA by TS provides a noninvasive tool for detection of tumor-derived mutations and mechanisms of PARPi resistance that may aid in directing patients to appropriate therapeutic strategies. With cfDNA fragmentation analyses, CHIP was identified in several patients and warrants further investigation.

## Introduction

Ovarian cancer is the second leading cause of death from gynecologic malignancies worldwide (1) and is usually diagnosed in advanced stages. Despite initial response to chemotherapy, approximately 70% of patients will relapse within 3 years and ultimately die from the disease (2). High-grade serous ovarian cancer (HGSOC) represents the most common subtype of epithelial ovarian cancer. HGSOC is characterized by severe genomic instability with universal *TP53* mutations (97%). Defects in homologous recombination DNA repair pathways are found in half of tumors; mutations in *BRCA1/2* account for 25% (15%–20% germline and 5%–10% somatic) of cases (3, 4).

Since the discovery that PARP inhibition causes synthetic lethality in *BRCA1/2* mutated tumors (5), PARP inhibitors (PARPi) have become standard of care in HGSOC. Olaparib, niraparib, and rucaparib were initially approved in the recurrent setting (6–8) and have moved earlier as maintenance therapies in the treatment paradigm. Currently, in the first-line maintenance setting, olaparib has shown clinical benefit in progression-free survival (PFS) and overall survival (OS) in tumors harboring *BRCA1* or *BRCA2* mutations and in combination with bevacizumab in tumors with homologous recombination deficiency (HRD). Niraparib has shown to meaningfully improve clinical outcomes in HRD tumors, and rucaparib provides benefit regardless of HRD status (9–11).

Maintenance therapy with PARPi provides impressive clinical benefit in patients that initially respond to platinum; however, drug resistance eventually emerges. Multiple mechanisms of PARPi resistance have been described, including restoration of homologous recombination repair pathways, replication fork protection, upregulation of cellular drug efflux pumps and reduction in PARP1 activity, among others (12). Identifying mechanisms of primary and acquired resistance is key to guide treatment and prevent recurrence on PARPi.

No standard treatment has been established for post-PARPi progression. In the OReO clinical trial (NCT-03106987), rechallenge with PARPi olaparib in patients with platinum-sensitive relapse progressing after one prior line of PARPi maintenance led to a modest improvement in PFS compared with placebo (PFS of 4.3–5.3 months and 2.8 months in treatment and control populations, respectively),

[1]Princess Margaret Cancer Centre, University Health Network, Toronto, Ontario, Canada. [2]Department of Medicine, University of Toronto, Toronto, Ontario, Canada. [3]Ontario Institute for Cancer Research, Toronto, Ontario, Canada. [4]Gynaecologic Cancer Programme, Vall d'Hebron Institute of Oncology (VHIO), Hospital Universitari Vall d'Hebron, Vall d'Hebron Barcelona Hospital Campus, Barcelona, Spain. [5]Department of Medical Biophysics, University of Toronto, Toronto, Ontario, Canada.

S. Lheureux and S.D. Prokopec contributed equally to this article.

**Corresponding Author:** Trevor J. Pugh, Princess Margaret Cancer Centre, University Health Network, MaRS Centre, 101 College Street, Toronto, Ontario, M5G 1L7, Canada. Phone: 416-946-2000; E-mail: trevor.pugh@utoronto.ca

Clin Cancer Res 2023;29:3706–16

**doi:** 10.1158/1078-0432.CCR-23-0797

## Translational Relevance

Targeted sequencing of cfDNA is a noninvasive tool that can identify emerging mechanisms of resistance to PARPi, including *BRCA1/2* reversion mutations that can impact response to further therapy. As HGSOC is a heterogeneous disease, testing of cfDNA can guide treatment decisions, particularly when tumor tissue is not readily available. Fragment size of cfDNA may be used to classify mutations as having tumor or nontumor origin and may be predictive of patient outcome, requiring further validation. In addition, cfDNA fragmentation profiles can differentiate potential CHIP mutations from tumor-derived variants in the absence of paired peripheral blood mononuclear cells (PBMC). Methods for variant detection using ctDNA are rapidly evolving and embedding into clinical trials for disease monitoring and patient selection.

regardless of *BRCA1/2* mutation status (13). In the phase II EVOLVE study, evaluating cediranib [a vascular endothelial growth factor (VEGF) receptor tyrosine kinase inhibitor] plus olaparib combination after progression on PARPi alone, objective responses were observed in three of 34 heavily pretreated patients (including two patients with platinum-resistant tumors and one patient who progressed on standard chemotherapy after PARPi progression) and showed a diversity of PARPi resistance mechanisms (14). The most common, acquired genomic alterations found at PARPi progression, were reversion mutations in homologous recombination (HR) genes *BRCA1*, *BRCA2*, and *RAD51B*; amplifications of *CCNE1*; and gene expression changes in *ABCB1* upregulation and *SLFN11* downregulation (14). Patients with reversion mutations in HR genes and/or *ABCB1* upregulation had the poorest outcomes, highlighting the need to identify these patients early, as they will no longer benefit from PARPi once these changes develop.

Detection of cancer-derived mutant fragments in blood cell–free DNA (cfDNA) has emerged as a potentially promising biomarker to monitor response to treatment, assess the development of drug resistance, and quantify minimal residual disease. Previous studies have reported a high concordance between mutational profiles in matched tumor tissue and blood cfDNA (15). Importantly, detection of *BRCA1/2* reversions in cfDNA is feasible in patients with HGSOC, and these reversions correlate with resistance to PARPi (16, 17). Here, we aim to evaluate the feasibility of using longitudinal cfDNA sequencing as a less invasive approach to identify emerging mechanisms of resistance to PARPi following progression, as well as during and after addition of cediranib as part of the EVOLVE trial (14). In addition, we will describe the concordance between genomic alterations identified in matched tumor biopsy and cfDNA at baseline.

# Materials and Methods

### Study design and participants

The proof-of-concept EVOLVE study (NCT-02681237), a multicenter open-label single-arm, assessed cediranib–olaparib combination therapy after progression on PARPi. Women with HGSOC and evidence of disease progression post PARPi were enrolled in one of three cohorts: platinum-sensitive after PARPi, platinum-resistant after PARPi, or progression on standard chemotherapy after progression on PARPi (exploratory; ref. 14). Written informed consent was obtained from patients, and the study was conducted in accordance with the Declaration of Helsinki and approved by an institutional review board. Study representation of underserved communities is available in Supplementary Table S1.

### Procedures

Blood plasma was isolated from peripheral blood samples at three different timepoints for all patients: baseline (PARPi progression), before second cycle (C2) of treatment (after the first cycle of olaparib–cediranib) and at the end of treatment (EOT) (progression on olaparib–cediranib or withdrawal due to adverse events; Supplementary Table S2). cfDNA was extracted from blood plasma using the QIAamp Circulating Nucleic Acid Kit (Qiagen) and quantified using the Qubit dsDNA HS Assay Kit (Thermo Fisher Scientific), as described previously (18).

### Design of targeted panel

To capture mechanisms of resistance specific to patients with ovarian cancer, we combined an existing cfDNA panel design (CHARM; ref. 19) targeting exons of *BRCA1*, *BRCA2*, *PALB2*, *TP53*, *APC*, *EPCAM* (including the 3′-UTR), *MLH1*, *MSH2*, *MSH6*, *PMS2*, 173 MSI loci as well as 44 single-nucleotide polymorphisms (SNP) and three sex-associated genes to confirm sample identity, with a newly designed panel named EVOLVE (Supplementary Table S3). The EVOLVE panel design includes all the above content from the CHARM panel and augments it with probes designed to capture introns of *BRCA1* and *BRCA2* to enable comprehensive detection of *BRCA1/2* reversions, intron 1 of *ABCB1* [most likely to participate in translocations to enable detection of gain-of-function structural variants (SV)] and all exons of *CCNE1* to enable detection of *CCNE1* amplifications. This study focuses on variants in *TP53, BRCA1, BRCA2, PALB2, CCNE1*, and *ABCB1*.

### Sequencing

Twenty nanograms of cfDNA was used for preparation of targeted sequencing libraries. Precapture libraries were prepared using KAPA DNA HyperPrep Kit (Roche, Catalog No. 07962363001) using IDT xGen Duplex Seq Adapter – Tech Access (IDT, Catalog No. 1080799). Target capture with the EVOLVE-CHARM hybrid-capture panel was performed using IDT xGEN Hybridization and Wash Kit (IDT, Catalog No. 1080584) and IDT xGEN Universal Blockers – TS mix (IDT, Catalog No. 1075475) according to the manufacturer's instructions. Prepared libraries were quantified using KAPA Library Quantification Kit (Roche, Catalog No. 7960336001). Libraries were balanced, pooled, and loaded on an Illumina NextSeq 550 Sequencing System (Illumina, Catalog No. SY-415–1002) and sequenced at 2×75 cycles to a minimum uncollapsed coverage of 20,000×.

### Data processing

Consensus bam files were produced from FASTQs using ConsensusCruncher (RRID:SCR_023654; ref. 20). Variant detection was performed individually on single-strand consensus sequences (SSCS), duplex consensus sequences (DCS), and all unique bam files. The final outputs were combined, and variants detected in multiple bam files were collapsed on the basis of level of evidence (all unique > DCS > SSCS).

Short somatic variants, including single-nucleotide variants (SNV) and short insertion/deletion events (INDEL), were called using an ensemble approach. Briefly, variants were called using MuTect (v1.1.5; RRID:SCR_000559), MuTect2 (GATK v3.8; RRID:SCR_001876), Strelka (v2.9.10; RRID:SCR_005109), VarScan (v2.4.2; RRID:SCR_006849), VarDict (v1.7.0; RRID:SCR_023658), and Pindel (v0.2.5b8; RRID:SCR_000560) using default (or author recommended)

parameters for targeted panels. Germline variants, as identified by previous whole-exome sequencing (WES) of patients' matched normal buffy coat cells (14), were removed. All variants called by MuTect2, or those called by three or more other tools were used in the final analysis. The final set of variants was annotated using vcf2maf (v1.6.17; ref. 21) and VEP (v98; RRID:SCR_007931; ref. 22) and contrasted to known somatic variants identified from prior WES of the baseline tumor tissue (14). Variants not observed in matched tissue were further annotated with clinical significance using ClinVar (RRID:SCR_006169) and OncoKB (RRID:SCR_014782). Any variant deemed pathogenic or likely pathogenic by ClinVar or found in OncoKB was carried forward as a "novel" variant. Copy-number status for targeted intervals was assessed using panelCN.mops (v1.14.0; RRID:SCR_023657), using diploid samples (those with two or fewer variant-containing reads at known somatic mutation sites) to generate a "normal" profile. SV were called using Delly (v0.8.1; RRID:SCR_004603), Manta (v1.6.0; RRID:SCR_022997), and SViCT (v1.0.1; RRID:SCR_023656) with candidate variants further merged and validated by MAVIS (v2.2.5; RRID:SCR_023655). SV validated by MAVIS were filtered to those with both breakpoints within target regions and to remove short deletions (<500 bp), as these frequently corresponded to gaps between adjacent target regions.

### Statistical analysis and data visualization

ctDNA content was determined using known *TP53* mutation status from the bulk tumor by force-calling allele counts at these positions using bam-readcount (v0.7.4; RRID:SCR_023653; minimum base quality score >10) or, where no known *TP53* mutation is available, using the maximum VAF across high-confidence somatic variants. Change in ctDNA content (ΔctDNA) was calculated as the relative percent difference between ctDNA content at screening and cycle 2 timepoints. Change in CA-125 levels were similarly calculated as the relative percent difference between CA-125 measurements (U/mL) at screening and cycle 2 of treatment. *BRCA1* and *BRCA2* reversions were detected by contrasting known mutations from the bulk tumor (germline and somatic) with the corresponding region of the cfDNA at each timepoint. Statistical analyses and visualizations were performed in the R statistical environment (v4.1.0). Survival analyses were performed using Cox proportional-hazards models [survival package for R (v3.2–11)]. Visualizations were generated using the BPG package (v6.0.3; RRID:SCR_023652), with lattice (v0.20–44; RRID:SCR_015662) and latticeExtra (v0.6–29) or ggplot2 (RRID:SCR_014601) package in R.

### Data availability

The primary sequence data generated in this study are not publicly available, as this is a legacy protocol for which patients did not consent to sharing of primary sequence data in controlled-access sequence databases. However, processed sequence data and secondary variant calls reported in this article may be available upon reasonable request from the corresponding author. All scientific computing code for the tertiary analysis and to reproduce all figures can be found at https://github.com/pughlab/EVOLVE_ctDNA.git.

## Results

Blood samples were collected from 30 of the 34 patients enrolled in the EVOLVE study: 11 in the platinum-sensitive, eight in platinum-resistant, and 11 in the exploratory cohort. For each patient, 20 to 2,074 ng (mean, 148 ng) of cfDNA was isolated from 7 mL (1–10 mL) of plasma and sequenced from samples collected before treatment (baseline – time of PARPi progression), on cycle 2 of treatment (on-treatment), and when available, at the end of treatment (EOT) with cediranib plus olaparib. This yielded a set of 28 pretreatment, 22 on-trial, and 28 EOT samples, for a total of 78 samples (**Fig. 1**; Supplementary Table S2). These samples were sequenced to a target coverage of 20,000× (range, 1,441–28,423×; median = 9,980×) using the CHARM+EVOLVE panel (Supplementary Table S3). The theoretical limit of detection (LOD) for reporting of SNV/INDELs in cfDNA was determined to be 1% [variant allele fraction (VAF) = 0.01] based on a mean collapsed coverage of 400× and minimum read support of 3. To confirm this for the CHARM+EVOLVE panel, a dilution series was performed using an in-house pool of reference cfDNA; all expected SNV/INDELs were detected down to a VAF of 0.5% (Supplementary Fig. S1A). Using a similar dilution series, the LOD for copy-number amplifications in cfDNA was 10% estimated tumor fraction (Supplementary Fig. S1B). Together, this cfDNA panel provides comprehensive coverage of the mechanisms of resistance discovered in the tumor tissue analyses from the EVOLVE trial (14).

### Inferring circulating tumor DNA content using somatic mutations

The circulating tumor DNA (ctDNA) fraction of cfDNA was estimated at each timepoint from force-called variant allele fractions of known *TP53* mutations (those known from tumor tissue testing) where available, or the maximum among all high-confidence somatic mutations detected (**Fig. 2A**; Supplementary Fig. S2). At baseline, 25 (of 28) samples had a known *TP53* mutation available to evaluate ctDNA levels; ctDNA levels ranged from 0.2% to 67% (median = 3.25%) of the total cfDNA. Samples with high ctDNA levels (>20%, $n = 5$) tended to have copy-number amplifications of *TP53* in matched tumor tissue ($n = 4$), potentially inflating tumor content estimates when relying on single mutations. There was no difference in baseline ctDNA levels among patients based on platinum sensitivity, best radiologic response based on RECISTv1.1, age at diagnosis, or final number of treatment cycles completed (Kruskal–Wallis tests or Spearman correlation; all $P > 0.1$; Supplementary Fig. S3A). However, patients with high ctDNA levels at baseline (>15%, $n = 6$) had a higher sum of targeted lesions in baseline CT scans compared with patients with low ctDNA levels (Wilcoxon rank-sum test $P = 0.043$; Supplementary Table S4). ctDNA levels in the on-treatment and EOT samples did not differ among patient groups, but ctDNA levels in EOT samples were frequently lower among patients with germline *BRCA1/2* mutations (Kruskal–Wallis $P = 0.048$) and decreased with higher number of treatment cycles (Spearman $\rho = -0.44$; $P = 0.026$), possibly relating to reduced tumor burden in these patients. Three patients had no known *TP53* mutation nor any detectable mutations in any cfDNA sample and ctDNA levels could not be estimated for these cases.

To evaluate whether treatment outcome was associated with changes in ctDNA levels over time, we compared ctDNA levels between pre- and on-treatment samples (ΔctDNA; **Fig. 2B**). Of the 18 patients with cfDNA collected at baseline and cycle 2 of treatment, 11 (61%) showed a 6% to 90% reduction over baseline ctDNA levels (median = 65% reduction), whereas seven (39%) patients showed a 13% to 296% increase (median = 85%) in ctDNA levels over time. Change in ctDNA levels was not associated with cohort, patient age at diagnosis, best response, or the overall number of cycles completed (**Fig. 2B**; Supplementary Fig. S3B) and was not associated with PFS (Supplementary Fig. S3C). ΔctDNA was correlated with changes in CA-125 levels using measurements collected at the same baseline and

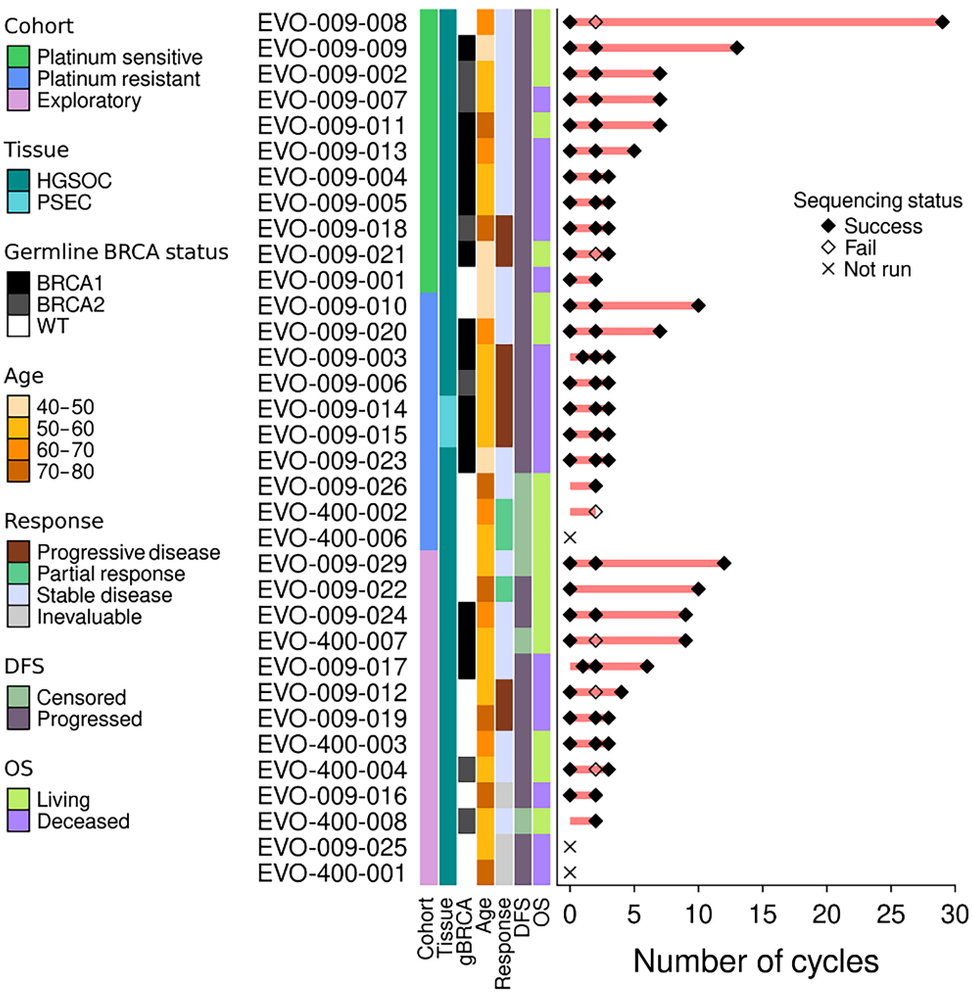


**Figure 1.**

Summary of patients with HGSOC. Summary of patient timelines; diamonds indicate time points at which samples were collected; empty points indicate the sample failed to provide sufficient cfDNA for sequencing, whereas each X indicates patients for which cfDNA was not obtained.

cycle 2 timepoints (Pearson correlation = 0.73; $P$ = 0.0006). Two patients demonstrated complete clearance of ctDNA, with no mutations detectable in the on-treatment cfDNA samples despite being detected at baseline. These patients (EVO-009–011 and EVO-009–017) were among those with longer times to progression, with 7.6 and 5.4 months, respectively (median = 2.4 months across the study cohort).

As we could not estimate ctDNA levels for all samples using mutations alone, we next examined their fragmentation profiles, as ctDNA frequently consists of shorter DNA fragments (∼150 bp) than normal cfDNA (∼167 bp corresponding to nucleosomal DNA; ref. 23). Overall, cfDNA from the study patients had a higher proportion of short (<150 bp; median proportion, 0.18) and long (250–320 bp; median proportion, 0.04) fragments compared with a panel of 23 healthy control individuals without cancer ($\text{median}_{\text{short}}$ = 0.15; $\text{median}_{\text{long}}$ = 0.01; **Fig. 3A**). cfDNA collected at baseline and EOT had a significantly higher proportion of short fragments than cfDNA from healthy controls (**Fig. 3B**). Similarly, cfDNA from baseline and on-trial samples had a significantly higher proportion of long fragments (Supplementary Fig. S4A and S4B), which may correspond to a higher frequency of dinucleosomal fragments than cfDNA from healthy controls. However, these proportions of short and long fragments did not correlate with ctDNA content estimated from somatic mutations (Supplementary Fig. S4C).

To confirm whether these differences in fragmentation profiles are biological, rather than technical, we further refined our analyses to consider fragment profiles at known somatic mutation sites (across *TP53*, *BRCA1*, and *BRCA2*). The fragment size distribution of mutation-containing reads was significantly different from wild-type reads at all timepoints (Wilcoxon rank-sum tests, $P < 0.05$; **Fig. 3C**), with wild-type reads centered around 167 bp, and mutant reads showing a bimodal distribution with peaks below expected single- and dinucleosomal fragment sizes. Among 67 known somatic mutations (across 56 cfDNA samples), 29 showed statistically significant differences in fragment size distribution at these sites (Wilcoxon rank-sum tests, $P < 0.05$; 25 with shorter fragments and three with longer fragments). At baseline, samples with significant differences in fragment size distribution at mutation sites compared with wild-type sites (Wilcoxon test $P < 0.05$, regardless of direction) had shorter time to progression (HR, 4.8; 95% CI, 1.8–12.5; $P$ = 0.001; **Fig. 3D**).

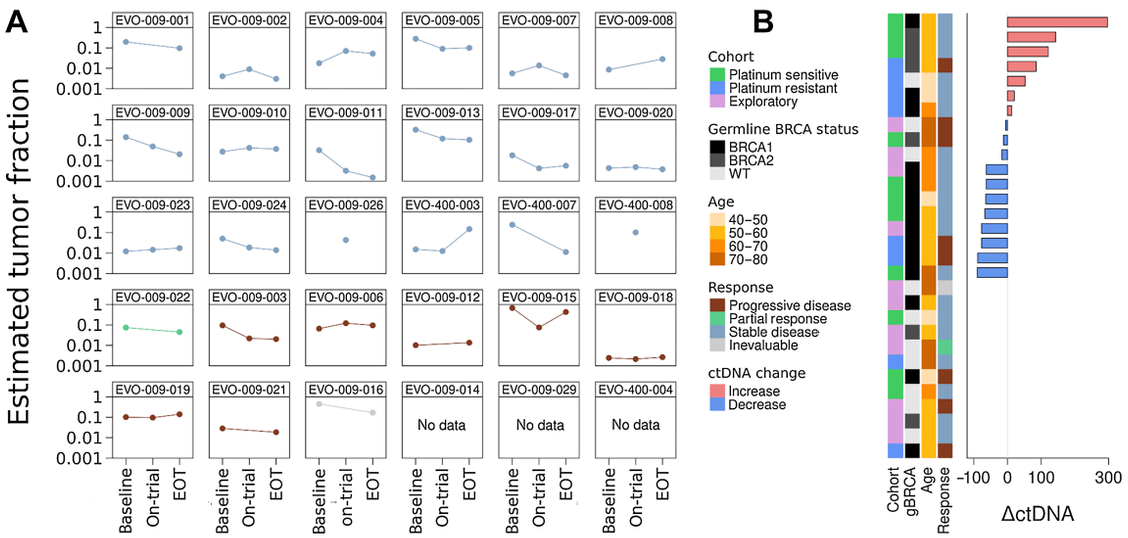


**Figure 2.**

Estimated tumor content of cfDNA. **A,** Estimated tumor-derived DNA fraction in cfDNA at each timepoint, based on allele fraction of known *TP53* mutations (or maximum VAF of high-confidence somatic variants); estimates for three patients could not be obtained, as their tumors had no known *TP53* mutations, and no somatic variants were called in the cfDNA. For each patient, points are colored according to best RECIST1.1 response. **B,** Change in estimated tumor fraction of circulating DNA between baseline and on-treatment samples (ΔctDNA); calculated as the relative percent difference between baseline and cycle 2 of treatment and was available for 18 of 30 patients. EOT, end of treatment.

## Identifying mechanisms of prior PARPi resistance in cfDNA at baseline

To assess whether cfDNA could recapitulate mutations known from matched tumor tissue, we compared our cfDNA mutation profiles against those from matched WES of baseline tumor tissue (14), mapped to the footprint of the targeted panel (Supplementary Fig. S5). When considering 43 expected mutations identified by WES, 32 were found in at least one matched cfDNA sample for an overall sensitivity of 74.4%. Breaking this down by time point, sensitivity was 70.7% (29/41), 63.3% (19/30), and 65.9% (27/41) in baseline, on-trial and EOT samples, respectively (**Fig. 4**). Of the 11 mutations we could not detect, five (11.6%) were in cfDNAs with inferred tumor content <1%.

We next searched for reversion mutations in *BRCA1* and *BRCA2*, as these are frequent mechanisms of resistance that can develop during treatment with PARPi. We found three reversion mutations (two in *BRCA1* and one in *BRCA2*) in cfDNA, and all three were previously detected in matched tumor tissue (**Table 1**; ref. 14); no novel reversion mutations were detected. Patient EVO-009–001 had a somatic frameshift deletion in exon 10 of *BRCA1* in a diagnostic tumor sample, which is partially excised in subsequent tumor samples by a larger deletion, which is also detected in baseline and EOT cfDNA samples (Supplementary Fig. S6A). Patient EVO-009–006 had a germline nonsense mutation in *BRCA2*, which reverted to a silent mutation in all tumor samples (Supplementary Fig. S6B). This silent reversion mutation was detected in cfDNA from this patient at all timepoints and increased in frequency over time (VAF = 0.021, 0.040, 0.043 in baseline, on-treatment, and EOT samples). Patient EVO-009–013 had a somatic frameshift deletion neighboring a germline frameshift deletion, which may result in a frame-corrected sequence (Supplementary Fig. S6C). This somatic mutation was detected in cfDNA at baseline (VAF = 0.155), but not in the on-treatment or EOT samples (despite VAF of 0.024 and 0.028 in the on-trial and EOT cfDNAs observed on manual inspection of mapped reads for these samples, likely due to lower coverage in these samples and the clustered nature of these events confounding our mutation callers). Of the remaining expected reversions, patient EVO-009–023 had a germline nonsense mutation in *BRCA1* excised by a 15-bp in-frame deletion in the baseline tumor that was not detected in cfDNA, and patient EVO-009–003 had a germline frameshift deletion in *BRCA1* predicted to be circumvented by a subclonal splice-site mutation in the baseline tumor that was not found in cfDNA. There was no read support for either of these mutations at any timepoint despite a median coverage of 1975× (1315–4590×).

We also searched for *CCNE1* amplifications as another potential indicator of PARPi resistance. On the basis of previous WES of matched baseline tumor samples, we expected six patients to have *CCNE1* amplifications. These were confirmed in the baseline ctDNA from two patients and baseline and EOT cfDNA from one patient using the EVOLVE panel. We further detected a *CCNE1* amplification in the baseline cfDNA for one patient that was not found in the tumor tissue (**Fig. 4**; Supplementary Fig. S7). This low detection rate is unsurprising, given the sequencing panels' LOD of 10% and the low tumor DNA content of these samples. Using this *CCNE1* amplification status, we compared fragment sizes of reads aligned to *CCNE1* between sample groups (amplified vs. nonamplified). We found samples with *CCNE1* amplifications had a higher ratio of short (90–150 bp) to normal (151–230 bp) fragments than non-*CCNE1* amplified samples (Wilcoxon rank-sum test; $P = 0.048$).

## Identifying novel variants in cfDNA that arise during treatment

In addition to mutations known from matched baseline tissue WES, we also sought to identify novel genomic alterations that arose throughout the course of treatment and may represent additional mechanisms of resistance while under combination cediranib and olaparib treatment. We identified 10 novel mutations across cfDNA from five patients that were not detected in baseline tumor tissue by

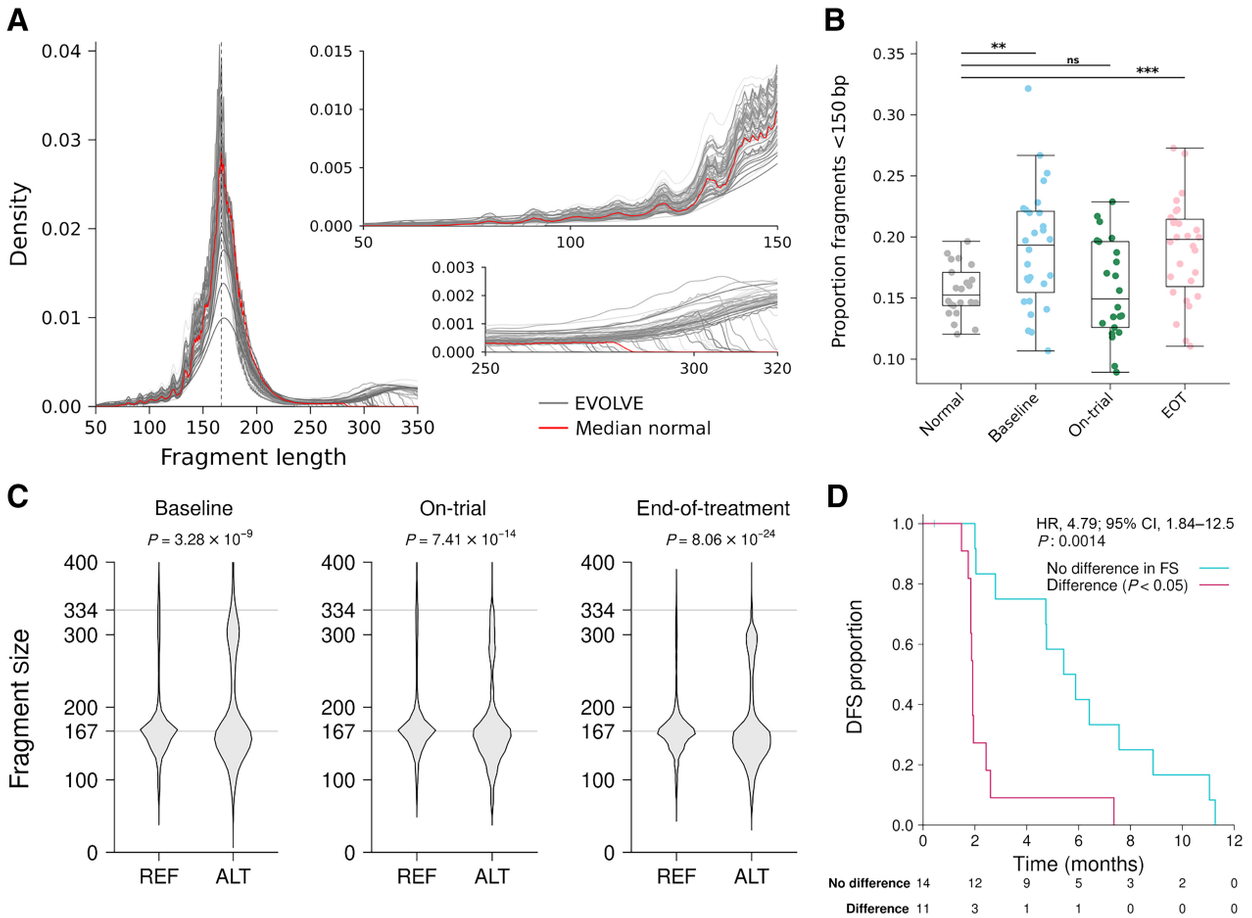


**Figure 3.**

Fragmentation profiles of cfDNA during treatment. **A,** Distribution of fragment size across all patient-derived and healthy control cfDNA samples. Each line represents the density (y-axis) of fragments at each size (x-axis; measured in nucleotide counts); each grey line represents a distinct patient-derived sample, whereas the red line shows the median profile across healthy controls. Insets show the increased frequency of short (100–150 bp) or long (250–320 bp) fragments in patient-derived samples. **B,** Patient-derived samples collected at baseline and time of progression show a higher proportion of short (<150 bp) fragments than healthy controls (two-sample Wilcoxon test: *, $P < 0.1$; **, $P < 0.01$; ***, $P < 0.001$), whereas samples collected at cycle 2 of treatment did not. **C,** Fragment size of mutation-containing reads is significantly different [frequently shorter (<150 bp) or longer (>230 bp), representing increased fragmentation beyond single- and dinucleosomal DNA sizes of 167 and 334 bp] than reads containing the reference allele at known somatic mutation sites (paired Wilcoxon rank-sum test). **D,** Kaplan–Meier curve showing disease-free survival for patients with a significant difference in mutation-specific fragmentation as compared with patients with no difference in mutation-specific fragmentation profiles [Cox proportional hazards test: HR, 4.8 (1.8–12.5), $P = 0.001$].

WES, including mutations in *TP53*, *BRCA2*, and *PALB2* (**Fig. 4**; Supplementary Table S5). However, we did not detect any new reversion mutations within the on-trial or EOT cfDNAs.

Two patients had notable driver mutations detectable in cfDNA that were missed by tissue WES testing. In cfDNA from EVO-400–007, we found a *BRCA2* p.E1734K mutation (VAF = 0.09 in baseline cfDNA but not detected in the EOT cfDNA) and two distinct *PALB2* frameshift mutations. *PALB2* p.G232Vfs*6 was detected in both the baseline and EOT cfDNA (VAF = 0.11 and 0.03, respectively) whereas p.R516Efs*45 was detected in the baseline cfDNA only (VAF = 0.10). EVO-400–007 had no *TP53* mutation known from tissue WES, however, we did detect a *TP53* p.R273H mutation with high frequency in the baseline cfDNA (VAF = 0.24) and low frequency in the EOT sample (VAF = 0.01). EVO-400–007 received nine cycles of treatment before progression, however, there was no on-treatment cfDNA available for this patient. Similarly, EVO-400–003 did not have an expected *TP53* mutation from tissue WES, yet we found a *TP53* p.R273C variant that increased in frequency at EOT (VAF = 0.02, 0.01, and 0.15 in the baseline, on-trial, and EOT cfDNAs), which corresponded with the patient's rapid clinical progression. Together, these cases show the potential of novel variant detection (rather than targeted variant detection) using cfDNA.

Three patients with known *TP53* variants from matched WES that were recapitulated in cfDNA were also found to carry novel, low-frequency *TP53* mutations. In addition to a *TP53* p.C135W mutation known from tissue WES, cfDNA from EVO-009–003 contained two other *TP53* mutations: p.R267W and p.I195T both had VAFs of 1%, consistent with the low ctDNA level of these samples (based on the known *TP53* p.C135W mutations; ctDNA level = 9%, 2%, and 1.5% for baseline, on-trial, and EOT respectively). Likewise, in addition to a known p.R196* variant, EOT cfDNA from EVO-009–008 also had *TP53* p.H214R and p.V272M variants detected (VAFs = 0.012 with a ctDNA level = 2%; ctDNA level for baseline sample was <0.5%). Finally, EVO-009–024 had both a known *TP53* p.X307 (splice site)

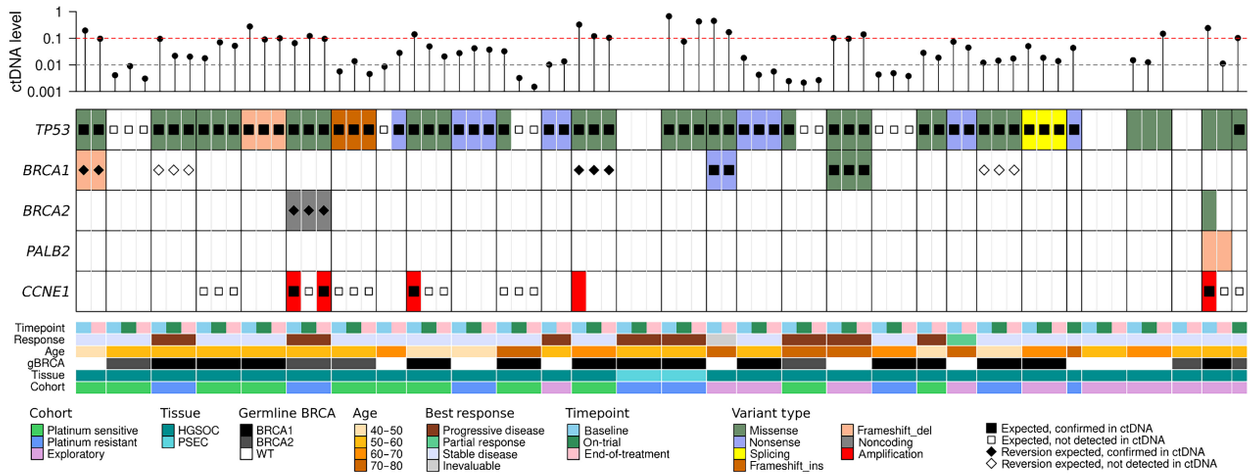


**Figure 4.**

Mutation summary of tumor-derived cfDNA. Somatic mutations were detected in *TP53*, *BRCA1*, *BRCA2*, and *PALB2* using an ensemble approach, whereas *CCNE1* amplifications were detected using panelCN.mops; symbols indicate mutation was expected on the basis of previous WES of the baseline tumor (filled = successfully detected; empty = not detected; diamonds represent previously identified reversion mutations). Top plot shows estimated ctDNA level for each sample with dashed lines to represent limits of detection for mutations (black) and copy-number changes (red).

variant and a novel *TP53* p.R280G mutation detected in the EOT cfDNA at similar frequencies (VAF = 0.01 for both; ctDNA level = 5%, 1%, and 1% for baseline, on-trial, and EOT cfDNA). None of these novel mutations were detected in the bulk tumor by WES.

It is possible that some of these "novel" *TP53* mutations are due to clonal hematopoiesis of indeterminate potential (CHIP) relating to the heavily pretreated condition of these patients, many of whom have undergone numerous rounds of prior platinum- and/or chemotherapies, including prior PARPi (24). To check this, we examined the fragment size of reference and variant-containing reads for each of these mutations to distinguish between tumor-derived and nontumor-derived cfDNA, as tumor-derived cfDNA has been shown to have a different fragmentation profile than CHIP cfDNA (25). We found five of the seven novel *TP53* mutations had normal-like fragmentation profiles (with median fragment sizes between 151–230 bp and no statistical difference between variant and wild-type reads; Wilcoxon rank-sum test $P > 0.1$), consistent with the CHIP hypothesis. The remaining two variants had statistically shorter fragments than wild-type reads: *TP53* p.H214R in EVO-009–008 at EOT (Wilcoxon rank-sum test, $P = 8.2\times10^{-8}$, median ALT fragment size = 146 bp) and *TP53* p.R273C in EVO-400–003 (Wilcoxon rank-sum tests <0.05; median ALT = 153 bp, 161 bp, and 156 bp in baseline, on-trial, and EOT respectively), consistent with tumor-derived cfDNA. In comparison to fragmentation profiles for germline variants in cfDNA from a cohort of healthy controls (**Fig. 5A**) and known somatic *TP53* mutations from our cohort (**Fig. 5B**), these suspected CHIP variants (**Fig. 5C**) resembled germline variants, whereas the remaining "novel" *TP53* mutations (**Fig. 5D**) had significantly different size distributions, akin to true somatic variants. Caution should be exercised when interpreting secondary TP53 mutations in cfDNA, especially in patients who are at risk of CHIP unrelated to ovarian cancer. However, it is possible to differentiate these mutations using fragmentation analysis.

Finally, we searched for SV within our cohort as another possible mechanism of resistance. We identified 29 SV (range, 1–3 SV per sample); eight of these were small (~565 bp) frameshift deletions around exons 1 to 3 of *CCNE1* that were also observed by CNA analysis (Supplementary Fig. S7). Translocations involving intron 1 of the *ABCB1* gene, which can lead to gain of function in ovarian cancer (26), were not detected in any sample. Two patients had clinically relevant intragenic deletions in *BRCA1* detected in cfDNA, including an 857-bp deletion within *BRCA1* in EVO-009–001 that encompasses a somatic *BRCA1* p.L631Qfs*4 variant and is classified as a reversion event (Supplementary Fig. S6A) and a 16-kbp duplication event in EVO-009–015 that encompasses exons 10 to 12 (Supplementary Fig. S6D). The remaining 19 SV could not be confirmed on manual inspection using Integrative Genomics Viewer (IGV; RRID:SCR_011793).

**Table 1.** Reversions as a mechanism of PARPi resistance detectable in cfDNA.

| Sample (WES) | Gene | Initial mutation | Reversion mutation (VAF in exome) | Findings in cfDNA |
|---|---|---|---|---|
| EVO-009–001-Bx | *BRCA1* | Somatic p.L631Qfs*4[a] | c.1509_2366del; p.S425_C712fs | Confirmed in cfDNA (baseline and end of treatment) |
| EVO-009–006-Bx | *BRCA2* | Germline c.7480C>T | c.7480C>A (20% A allele) | Confirmed in cfDNA (baseline, on-trial and time of progression) |
| EVO-009–013-Bx | *BRCA1* | Germline c.2999del | c.3008_3009del (31.0%) | Confirmed in cfDNA (baseline only); [a]most somatic callers discard this as too many clustered events on short reads |

Note: Somatic reversions previously detected in post-PARPi progressed tumor tissue using WES. Of these, three were successfully detected, and two had no evidence in cfDNA.

[a]Reversion detected but did not pass thresholds for high-confidence somatic mutation classification.

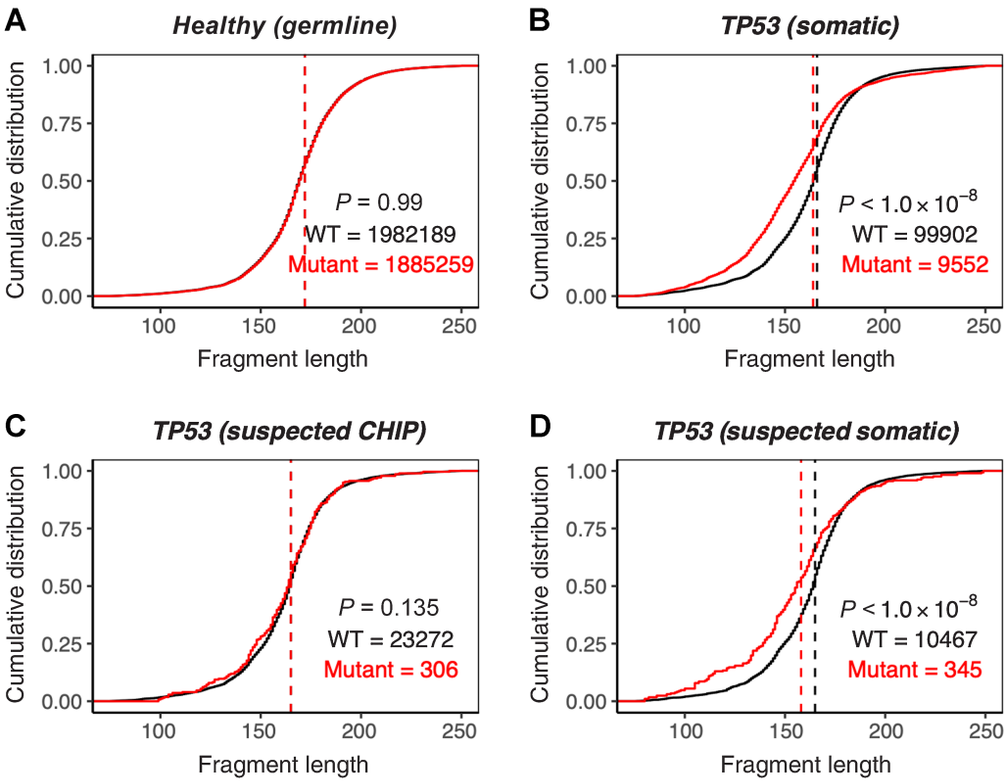


**Figure 5.**

Fragment size distribution of tumor and nontumor variants. Fragment size distributions of reference- and variant-containing reads for (**A**) germline SNP from a cohort of 22 healthy controls as well as (**B**) known somatic *TP53* mutations, (**C**) suspected CHIP TP53 mutations, and (**D**) novel somatic *TP53* mutations from our patient cfDNA. Distributions for reference- and variant-containing reads were compared using a one-sided KS test [alternative hypothesis = the cumulative distribution function (CDF) of variant fragment size is above, and therefore consists of shorter fragments, than the CDF of reference reads].

## Discussion

This is the first study to evaluate the feasibility of longitudinal cfDNA targeted panel sequencing with matched baseline tumor tissue to identify emerging mechanisms of resistance to PARPi over time in 30 patients with platinum-agnostic HGSOC treated with cediranib plus olaparib following progression on previous PARPi. Using our targeted CHARM+EVOLVE panel, we detected between zero and five somatic mutations (SNV/INDEL) per cfDNA sample. Across all timepoints, our cfDNA approach demonstrated an overall sensitivity of 74.4% to detect known mutations identified in tumor tissue WES. This sensitivity estimate is consistent with previous results by Oikkonen and colleagues, who reported a 79% concordance between mutations detected from cfDNA and tumor tissue samples from the same patient in a prospective cohort of 12 patients with ovarian cancer (27). In addition, the use of ctDNA identified new variants, not detected in matched baseline tumors.

High ctDNA levels (>15% of total cfDNA) were associated with a higher sum of targeted lesions in baseline CT scans suggesting a correlation between ctDNA levels and tumor burden. As suspected, changes in ctDNA levels correlated with changes in CA-125 measurements from baseline to cycle 2; however, neither metric correlated with best response or PFS, possibly due to the small sample size and low response rate observed in this study.

Interestingly, the fragmentation profiles of ctDNA at baseline were associated with PFS. Specifically, patients with mutation-containing fragments that differed significantly in size from matched reference-allele-containing fragments had shorter time to progression. Therefore, analyses of fragmentation profiles of cfDNA collected at baseline warrants further investigation.

Reversion mutations in *BRCA1* and *BRCA2* are the most described mechanisms of resistance to platinum and PARPi. In our previous analysis of the tumor WES data, we identified five *BRCA1/2* reversion mutations in tumor samples collected at the time of PARPi progression (24% of the 21 tumors with mutations in *BRCA1/2*; ref. 14). This rate of *BRCA1/2* reversions was consistent with a previous study by Lukashchuk and colleagues, which reported reversion mutations in 26% of patients with advanced ovarian cancer at the time of progression on olaparib (28). Using targeted sequencing of cfDNA, three out of five of these reversion mutations (two in *BRCA1* and one in *BRCA2*) were successfully detected, yet two reversions were missed, likely due to the low variant frequency of subclonal events (below the LOD of the panel) or limitations of the technology used (large INDELs on short reads). Targeted panel sequencing of cfDNA may not be as sensitive as tumor WES in this context. In similar studies, Christie and colleagues identified reversion mutations in ctDNA in three of five patients with reversion mutations detected in tumor tissue (16), whereas Lin and colleagues identified *BRCA1/2* reversion mutations in pretreatment ctDNA from eight of 112 patients, and four of these were confirmed in matched tumor biopsy (17). Although these studies demonstrate the utility of sequencing cfDNA to identify reversion mutations during PARPi therapy, particularly if those mutations are highly prevalent in

the tumor, difficulties persist for low frequency or subclonal variants; an issue compounded by low levels of ctDNA shed by HGSOC. Further, our cfDNA sequencing methodology used short reads (70 bp) leading to difficulties in aligning and detecting longer indels, such as one of our expected, but missed, reversion mutations (a 15-bp deletion). With the current techniques, sequencing of tumor tissue remains necessary for a comprehensive analysis; however, with the evolution from targeted panels to whole-genome sequencing, the sensitivity of variant calling in cfDNA will likely increase. Further, the use of cfDNA to detect these variants would avoid delays associated with biopsy booking, tissue annotation, and, importantly, is more safe and convenient option for patients.

Data regarding mechanisms of resistance to PARPi beyond *BRCA1/2* reversion mutations are scarce. Alterations in the cell-cycle pathway have been proposed as potential modulators of PARPi sensitivity (29). CCNE1 promotes cell-cycle progression through the $G_1$–S phase; its overexpression results in increased stress at replication forks and double-strand DNA breaks, leading to genomic instability. CCNE1 alterations have been associated with platinum resistance (30) and have been observed at PARPi progression; however, these alterations are currently challenging to detect in cfDNA. In our study, we detected three out of six expected *CCNE1* amplifications at baseline, suggesting deep sequencing of small, targeted panels is not sufficient to identify gene-level copy-number (CN) changes due to the low tumor fractions involved and high detection thresholds required for cfDNA. Identification of *CCNE1* overexpression is of clinical significance, as several studies are currently exploring this target to overcome drug resistance in ovarian cancer (31, 32). An alternative detection approach (such as shallow WGS of cfDNA, rather than deep sequencing of targeted regions) may be beneficial for samples with low ctDNA levels.

Using longitudinal cfDNA analysis, we identified multiple mutations not previously detected in baseline tumor WES, including seven low-frequency *TP53* mutations. In ovarian cancer, advanced age and a high number of prior platinum-based chemotherapy lines have been identified as risk factors to acquire CHIP-associated gene mutations. CHIP has been associated with an increased risk of developing hematologic malignancies and cardiovascular disease (33), and previous trials have linked preexisting *TP53* CHIP variants with therapy-related myeloid neoplasms after rucaparib treatment (24). As tumor-derived cfDNA molecules have a shorter size distribution compared with nontumor-derived cfDNA, which is of primarily hematopoietic origin (25, 34), we used fragmentation profiles to differentiate between tumor-derived variants and CHIP variants. This indicated that five out of seven of these novel *TP53* mutations (occurring in seven patients; 13% of the cohort) had fragmentation profiles suggestive of CHIP. None of these patients had evidence of myelodysplastic syndromes (MDS)/ acute myeloid leukemia (AML), and there was no enrichment for higher age or increased number of prior treatments. Importantly, due to the high depth of these sequencing experiments, a VAF threshold of ≥2% has been recommended for CHIP variants (35), yet the majority of our proposed cases are below this threshold. Fragmentomic analysis allowed us to further differentiate potential CHIP mutations from tumor-derived variants in the absence of paired peripheral blood mononuclear cell (PBMC) DNA.

Our study demonstrates that mechanisms of resistance are detectable by cfDNA, opening the door for using this technique to guide timely treatment decisions for patients with HGSOC, even if tissue is unavailable for serial testing. Detection of *BRCA1/2* reversion mutations in tissues from the EVOLVE study predicted poorer outcomes with further PARPi, thus their identification can trigger a change of treatment beyond PARPi (14). Recently, in the ARIEL-4 trial, translational studies have discovered that some patients who were treated with weekly paclitaxel experienced a decrease in the frequency of BRCA1/2 reversion mutations. This finding suggests that tumor subclones that possess these reversions are more susceptible to the effects of paclitaxel. As a result, these patients show heightened sensitivity to subsequent PARPi (32). Thus, monitoring for emergent resistance along disease trajectory may be important for timely treatment decisions, particularly delivery of new therapeutic approaches that could overcome or bypass resistance (currently under investigation in the REVOLVE study NCT-05065021). Naturally, further investigation is required to validate our findings and to improve sensitivity of cfDNA detection in HGSOC to inform timepoints of greatest clinical utility particularly in settings where multiple biopsies are not feasible.

In our study, 16 cfDNA samples had tumor fractions below our LOD for somatic variants; eight samples had no somatic mutations detected, suggesting the need for profiling beyond targeted panels. Zviran and colleagues proposed a WGS approach for cfDNA cancer monitoring that enables ultrasensitive detection and overcomes the limitation of ctDNA abundance (36). Mouliere and colleagues focused on differences in fragment lengths of cfDNA using low-pass WGS (0.4x); they found that selection of fragments between 90 and 150 bp improved detection of tumor DNA, with more than twofold median enrichment in >95% of cases (23). Combining these methods with lessons learned from our targeted panel sequencing study may enable algorithms for tissue-agnostic mutational sampling and fragmentomic analysis in the future.

Targeted sequencing of ctDNA is a useful, noninvasive method to identify potential mechanisms of PARPi resistance, albeit imperfectly due to low levels of cfDNA shed by HGSOC. Use of fragmentomics may allow for detection of CHIP, which can arise during treatment and requires further investigation. Moving from targeted panels to whole-genome sequencing that integrates mutational sampling, copy-number detection, and fragmentomics (36) will likely increase sensitivity and specificity required to guide therapeutic strategies in a timely manner for HGSOC.

## Authors' Disclosures

S. Lheureux reports grants from AstraZeneca during the conduct of the study; grants and personal fees from Roche, AstraZeneca, and GSK; grants from Repare Therapeutics; and personal fees from Eisai and Merck outside the submitted work. A. Oaknin reports personal fees and other support from F. Hoffmann-La Roche and PharmaMar; personal fees from ImmunoGen, Mersana Therapeutics, OneXerna Therapeutics, Inc., Regeneron, Sattuck Labs, Seagen, and Sutro Biopharma outside the submitted work. A. Madariaga reports personal fees from AstraZeneca, GSK, PharmaMar, Clovis, and MSD outside the submitted work. N.C. Dhani reports other support from Merck and Knight Therapeutics outside the submitted work. A.M. Oza reports PI and steering committee relationships with AstraZeneca, GSK, and Clovis and advisory board relationships with AstraZeneca and Morphosys. As a PI, A.M. Oza also reports receiving funding from peer-reviewed agencies such as the U.S NCI, Department of Defense, Cancer Care Ontario, Ontario Institute for Cancer Research, and Princess Margaret Cancer Foundation. T.J. Pugh reports personal fees from Merck, Chrysalis Biomedical Advisors, AstraZeneca, and SAGA Diagnostics and grants from Roche/Genentech outside the submitted work. No disclosures were reported by the other authors.

## Authors' Contributions

**S. Lheureux:** Conceptualization, resources, data curation, software, formal analysis, supervision, funding acquisition, investigation, visualization, writing–original draft, project administration, writing–review and editing. **S.D. Prokopec:** Conceptualization, resources, data curation, software, formal analysis, supervision, funding acquisition, investigation, visualization, writing–original draft, project administration, writing–review and editing. **L.E. Oldfield:** Software, methodology, writing–

review and editing. **E. Gonzalez-Ochoa:** Formal analysis, writing–original draft, writing–review and editing. **J.P. Bruce:** Conceptualization, software, formal analysis, supervision, methodology, writing–review and editing. **D. Wong:** Software, methodology, writing–review and editing. **A. Danesh:** Software, writing–review and editing. **D. Torti:** Data curation. **J. Torchia:** Data curation, formal analysis. **A. Fortuna:** Data curation, formal analysis. **S. Singh:** Data curation. **M. Irving:** Data curation. **K. Marsh:** Data curation. **B. Lam:** Data curation, writing–review and editing. **V. Speers:** Resources, supervision, writing–review and editing. **A. Yosifova:** Resources, supervision, writing–review and editing. **A. Oaknin:** Resources, project administration, writing–review and editing. **A. Madariaga:** Resources, writing–review and editing. **N.C. Dhani:** Resources, writing–review and editing. **V. Bowering:** Resources, project administration, writing–review and editing. **A.M. Oza:** Conceptualization, funding acquisition, project administration, writing–review and editing. **T.J. Pugh:** Conceptualization, resources, software, formal analysis, supervision, funding acquisition, investigation, methodology, project administration, writing–review and editing.

## Acknowledgments

We would like to thank the patients and their families for their participation and contributions to the EVOLVE clinical trial. This study was conducted with the support of the Ontario Institute for Cancer Research's Genomics Program (genomics.oicr.on.ca) and Translational Genomics Laboratory, a joint initiative between the Princess Margaret Cancer Centre and the Ontario Institute for Cancer Research. Thank you to Ozmosis for the study coordination support. T.J. Pugh holds the Canada Research Chair in Translational Genomics and is supported by a Senior Investigator Award from the Ontario Institute for Cancer Research and the Gattuso-Slaight Personalised Cancer Medicine Fund at the Princess Margaret Cancer Centre. S. Lheureux holds the Westaway Chair in Ovarian Cancer Research at Princess Margaret Cancer Centre. The study was supported by the Princess Margaret Foundation and OICR - Translational Research Initiative (TRI) Ovarian Cancer Grant.

The publication costs of this article were defrayed in part by the payment of publication fees. Therefore, and solely to indicate this fact, this article is hereby marked "advertisement" in accordance with 18 USC section 1734.

## Note

Supplementary data for this article are available at Clinical Cancer Research Online (http://clincancerres.aacrjournals.org/).

Received March 20, 2023; revised May 4, 2023; accepted June 14, 2023; published first June 16, 2023.

## References

1. Sung H, Ferlay J, Siegel RL, Laversanne M, Soerjomataram I, Jemal A, et al. Global cancer statistics 2020: GLOBOCAN estimates of incidence and mortality worldwide for 36 cancers in 185 countries. CA Cancer J Clin 2021;71:209–49.
2. Ledermann JA, Raja FA, Fotopoulou C, Gonzalez-Martin A, Colombo N, Sessa C. Newly diagnosed and relapsed epithelial ovarian carcinoma: ESMO clinical practice guidelines for diagnosis, treatment and follow-up. Ann Oncol 2013;24: vi24–32.
3. The cancer genome atlas research network. integrated genomic analyses of ovarian carcinoma. Nature 2011;474:609–15.
4. Norquist BM, Harrell MI, Brady MF, Walsh T, Lee MK, Gulsuner S, et al. Inherited mutations in women with ovarian carcinoma. JAMA Oncol 2016; 2:482.
5. Fong PC, Boss DS, Yap TA, Tutt A, Wu P, Mergui-Roelvink M, et al. Inhibition of poly(ADP-ribose) polymerase in tumors from *BRCA* mutation carriers. N Engl J Med 2009;361:123–34.
6. Pujade-Lauraine E, Ledermann JA, Selle F, Gebski V, Penson RT, Oza AM, et al. Olaparib tablets as maintenance therapy in patients with platinum-sensitive, relapsed ovarian cancer and a BRCA1/2 mutation (SOLO2/ENGOT-Ov21): a double-blind, randomised, placebo-controlled, phase 3 trial. Lancet Oncol 2017; 18:1274–84.
7. Mirza MR, Monk BJ, Herrstedt J, Oza AM, Mahner S, Redondo A, et al. Niraparib maintenance therapy in platinum-sensitive, recurrent ovarian cancer. N Engl J Med 2016;375:2154–64.
8. Coleman RL, Oza AM, Lorusso D, Aghajanian C, Oaknin A, Dean A, et al. Rucaparib maintenance treatment for recurrent ovarian carcinoma after response to platinum therapy (ARIEL3): a randomised, double-blind, placebo-controlled, phase 3 trial. Lancet North Am Ed 2017;390:1949–61.
9. Moore K, Colombo N, Scambia G, Kim B-G, Oaknin A, Friedlander M, et al. Maintenance olaparib in patients with newly diagnosed advanced ovarian cancer. N Engl J Med 2018;379:2495–505.
10. González-Martín A, Pothuri B, Vergote I, DePont Christensen R, Graybill W, Mirza MR, et al. Niraparib in patients with newly diagnosed advanced ovarian cancer. N Engl J Med 2019;381:2391–402.
11. Monk BJ, Parkinson C, Lim MC, O'Malley DM, Oaknin A, Wilson MK, et al. A randomized, phase III trial to evaluate rucaparib monotherapy as maintenance treatment in patients with newly diagnosed ovarian cancer (ATHENA–MONO/GOG-3020/ENGOT-ov45). J Clin Oncol 2022;40:3952–64.
12. McMullen M, Karakasis K, Madariaga A, Oza AM. Overcoming platinum and PARP-inhibitor resistance in ovarian cancer. Cancers 2020;12:1607.
13. Pujade-Lauraine E, Selle F, Scambia G, Asselain B, Marmé F, Lindemann K, et al. LBA33 maintenance olaparib rechallenge in patients (pts) with ovarian carcinoma (OC) previously treated with a PARP inhibitor (PARPi): phase IIIb OReO/ENGOT Ov-38 trial. Ann Oncol 2021;32:S1308–9.
14. Lheureux S, Oaknin A, Garg S, Bruce JP, Madariaga A, Dhani NC, et al. EVOLVE: a multicenter open-label single-arm clinical and translational phase II trial of cediranib plus olaparib for ovarian cancer after PARP inhibition progression. Clin Cancer Res 2020;26:4206–15.
15. Siravegna G, Marsoni S, Siena S, Bardelli A. Integrating liquid biopsies into the management of cancer. Nat Rev Clin Oncol 2017;14:531–48.
16. Christie EL, Fereday S, Doig K, Pattnaik S, Dawson S-J, Bowtell DDL. Reversion of *BRCA1/2* germline mutations detected in circulating tumor DNA from patients with high-grade serous ovarian cancer. J Clin Oncol 2017;35:1274–80.
17. Lin KK, Harrell MI, Oza AM, Oaknin A, Ray-Coquard I, Tinker AV, et al. *BRCA* reversion mutations in circulating tumor DNA predict primary and acquired resistance to the PARP inhibitor rucaparib in high-grade ovarian carcinoma. Cancer Discov 2019;9:210–9.
18. Bratman SV, Yang SYC, Iafolla MAJ, Liu Z, Hansen AR, Bedard PL, et al. Personalized circulating tumor DNA analysis as a predictive biomarker in solid tumor patients treated with pembrolizumab. Nat Cancer 2020;1: 873–81.
19. Wong D, Luo P, Oldfield L, Gong H, Brunga L, Rabinowicz R, et al. Integrated analysis of cell–free DNA for the early detection of cancer in people with Li-Fraumeni syndrome [Internet]. Genetic and Genomic Medicine; 2022. Available from: http://medrxiv.org/lookup/doi/10.1101/2022.10.07.22280848.
20. Wang TT, Abelson S, Zou J, Li T, Zhao Z, Dick JE, et al. High efficiency error suppression for accurate detection of low-frequency variants. Nucleic Acids Res 2019;47:e87.
21. Cyriac Kandoth. Vcf2Maf V1.5 [Internet]. Zenodo; 2015 [cited 2022 Oct 24]. Available from: https://zenodo.org/record/593251
22. McLaren W, Gil L, Hunt SE, Riat HS, Ritchie GRS, Thormann A, et al. The ensembl variant effect predictor. Genome Biol 2016;17:122.
23. Mouliere F, Chandrananda D, Piskorz AM, Moore EK, Morris J, Ahlborn LB, et al. Enhanced detection of circulating tumor DNA by fragment size analysis. Sci Transl Med 2018;10:eaat4921.
24. Kwan TT, Oza AM, Tinker AV, Ray-Coquard I, Oaknin A, Aghajanian C, et al. Preexisting *TP53*-variant clonal hematopoiesis and risk of secondary myeloid neoplasms in patients with high-grade ovarian cancer treated with rucaparib. JAMA Oncol 2021;7:1772.
25. Marass F, Stephens D, Ptashkin R, Zehir A, Berger MF, Solit DB, et al. Fragment size analysis may distinguish clonal hematopoiesis from tumor-derived mutations in cell–free DNA. Clin Chem 2020;66:616–8.
26. Christie EL, Pattnaik S, Beach J, Copeland A, Rashoo N, Fereday S, et al. Multiple ABCB1 transcriptional fusions in drug resistant high-grade serous ovarian and breast cancer. Nat Commun 2019;10:1295.
27. Oikkonen J, Zhang K, Salminen L, Schulman I, Lavikka K, Andersson N, et al. Prospective longitudinal ctDNA workflow reveals clinically actionable alterations in ovarian cancer. JCO Precis Oncol 2019;3: PO.18.00343.

28. Lukashchuk N, Armenia J, Tobalina L, Carr TH, Milenkova T, Liu YL, et al. BRCA reversion mutations mediated by microhomology-mediated end joining (MMEJ) as a mechanism of resistance to PARP inhibitors in ovarian and breast cancer. J Clin Oncol 40:5559.
29. Swisher EM, Kwan TT, Oza AM, Tinker AV, Ray-Coquard I, Oaknin A, et al. Molecular and clinical determinants of response and resistance to rucaparib for recurrent ovarian cancer treatment in ARIEL2 (parts 1 and 2). Nat Commun 2021;12:2487.
30. Patch A-M, Christie EL, Etemadmoghadam D, Garsed DW, George J, Fereday S, et al. Whole-genome characterization of chemoresistant ovarian cancer. Nature 2015;521:489–94.
31. Xu H, George E, Kinose Y, Kim H, Shah JB, Peake JD, et al. CCNE1 copy number is a biomarker for response to combination WEE1-ATR inhibition in ovarian and endometrial cancer models. Cell Rep Med 2021;2:100394.
32. Gallo D, Young JTF, Fourtounis J, Martino G, Álvarez-Quilón A, Bernier C, et al. CCNE1 amplification is synthetic lethal with PKMYT1 kinase inhibition. Nature 2022;604:749–56.
33. Jaiswal S, Fontanillas P, Flannick J, Manning A, Grauman PV, Mar BG, et al. Age-related clonal hematopoiesis associated with adverse outcomes. N Engl J Med 2014;371:2488–98.
34. Underhill HR, Kitzman JO, Hellwig S, Welker NC, Daza R, Baker DN, et al. Fragment length of circulating tumor DNA. Kwiatkowski DJ, editor. PLOS Genet 2016;12:e1006162.
35. Steensma DP, Bejar R, Jaiswal S, Lindsley RC, Sekeres MA, Hasserjian RP, et al. Clonal hematopoiesis of indeterminate potential and its distinction from myelodysplastic syndromes. Blood 2015;126:9–16.
36. Zviran A, Schulman RC, Shah M, Hill STK, Deochand S, Khamnei CC, et al. Genome-wide cell-free DNA mutational integration enables ultra-sensitive cancer monitoring. Nat Med 2020;26:1114–24.